PCCP

Accepted Manuscript

ROYAL SOCIETY OF CHEMISTRY

www.rsc.org/pccp

Journal Name

ARTICLE

Porous one-dimensional Mo_2C/amorphous carbon composites: high-efficient and durable electrocatalysts for hydrogen generation†

Received 00th January 20xx,
Accepted 00th January 20xx

DOI: 10.1039/x0xx00000x

www.rsc.org/

Kai zhang, Chunyan Li, * Yang Zhao, Xianbo Yu and Yujin Chen*

Porous one-dimensional Mo_2C/amorphous carbon composites were fabricated by *in-situ* solid state reactions for effective and high-performance electrocatalysts towards hydrogen evolution reaction (HER). The morphological and structural characteristics of the Mo_2C based electrocatalysts were analyzed by scanning electron microscopy (SEM), transmission electron microscopy (TEM), and X-ray diffraction (XRD). The analyses showed that they had various advantages for HER, including high crystallinity, porous and tubular characteristic and good conductivity. The porous one-dimensional Mo_2C/amorphous carbon composites with a larger content of Mo_2C and moderate thickness of the carbon layers exhibited superior catalytic activities for HER to most Mo_2C based electrocatalysts recently reported.

1 Introduction

With the increasingly consumption of traditional fossil fuels, the global energy crisis has been emerged. It has become crucial and urgent to seek sustainable and clean energy sources. Hydrogen, as a renewable energy carrier with high gravimetric energy density, has attracted significant attention. [1] Due to the characteristics of the possibility of being produced from electrochemical water splitting and the zero emission of global warming gases from hydrogen utilization, hydrogen is considered to be a promising candidate for traditional petroleum fuels in the future.[1]

To improve the efficiency of water splitting for hydrogen generation the active catalysts are required.[1] Although platinum has the excellent activity for HER, its scarcity, low abundance and high cost prevent their widespread applications. Therefore, it is quite desirable to search and exploit non-Pt HER catalysts with high catalytic activity, long-term stability and low cost. Molybdenum-based materials such as molybdenum disulfide (MoS_2),[2] molybdenum phosphide (MoP),[3] molybdenum nitride (MoN),[4,5] and molybdenum carbide (Mo_2C),[5-16] have been exploited as electrocatalysts for HER recently. But during the synthesis processes of these molybdenum-based materials some poisonous and harmful gases such as hydrogen sulfide, sulfur oxide, hydrogen phosphide, and ammonia, etc. were used or released. Recently, carbon black, carbon nanotubes (CNTs) and graphene can be used as the supporting substrates to grow Mo_2C nanostructures and the poisonous and harmful gases such as CO, C_2H_6 or CH_4 are not needed.[5-15] These carbon-supported Mo_2C materials with high conductivities exhibited remarkable catalytic activity and good corrosion resistance for HER in both acidic and basic conditions due to their similar electronic stuctures with Pt-group metals.[5-15] For example, β-Mo_2C nanoparticles inlaid or anchored into the carbon nanotubes (Mo_2C–CNT) synthesized by Chen *et al* exhibited superior electrocatalytic activity and stability in the HER compared to the bulk Mo_2C.[7] For driving cathodic current densities of 1 mA cm^{-2}, an overpotential is as low as 63 mV in 0.1 M $HClO_4$ solution.[7] On the basis of X-ray absorption analysis results, they attributed the enhancement to the electronic modification which makes the surface exhibit a relatively moderate Mo–H bond strength.[7]

Although many outstanding efforts have been made to exploit high-performance Mo_2C-based catalysts, a high current density achieved by them at low overpotential (η) is yet unsatisfactory. In this work, we fabricated porous one-dimensional (1D) Mo_2C/amorphous carbon composites by *in-situ* solid state reactions using MoO_3/polyaniline nanorod (MoO_3/PANI) hybrid as a precursor.[2g, 16-18] In order to optimize the HER activity of the catalysts, three Mo_2C-based electrocatalysts are fabricated and named as Mo_2C-1, Mo_2C-2 and Mo_2C-3, respectively (Experimental section). Notably, by adjusting the amount of PANI nanorods grown on the surface of MoO_3 nanorods, the thickness of the amorphous carbon layers, and the crystal size and the content of Mo_2C in porous 1D Mo_2C/amorphous carbon composites can be tuned. The electrochemical measurements show that Mo_2C-2 with a larger content of Mo_2C and moderate thickness of the carbon layers exhibit excellent HER activity, including a small onset overpotential, a Tafel slope of 57.5 mV $decade^{-1}$ and an exchange current density of 102.3 μA cm^{-2}. Especially, for driving cathodic current densities of 10 mA cm^{-2} in acidic

Key Laboratory of In-Fiber Integrated Optics, Ministry of Education, and College of Science, Harbin Engineering University, Harbin 150001, China. Fax: 86-451-82519754; Tel: 86-451-82519754; E-mail: chenyujin@hrbeu.edu.cn and chunyanli@hrbeu.edu.cn

†Electronic Supplementary Information (ESI) available: [Comparisons of HER performances among different Mo-based catalysts, R_{ct} values, Exchange current densities extracted from Tafel plots and Nyquist plots of Mo_2C-1, Mo_2C-2 and Mo_2C-3.]. See DOI: 10.1039/x0xx00000x

media, the Mo_2C-2 electrode only need overpotentials of 115 mV vs RHE, greatly lower than those of most Mo_2C based catalysts recently reported.

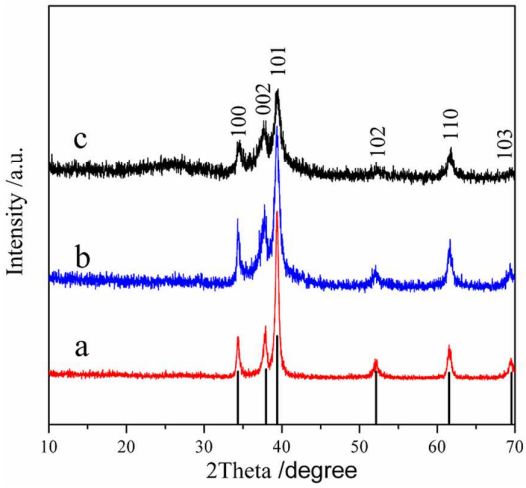

Figure 1. XRD patterns of Mo_2C-1 (a), Mo_2C-2 (b) and Mo_2C-3 (c).

2 Experimental

2.1 Synthesis of materials

Preparation of α-MoO_3 nanorods: 7.2 g of α-MoO_3 powder was reacted with 55mL of 30% aqueous H_2O_2 and dissolved completely under stirring. 27 mL of concentrated nitric acid and 170 mL distilled water were then added to the above solution. The mixture was kept for 4 days at room temperature. 35 mL of the mixture was then transferred into a Teflon-lined stainless steel autoclave with a capacity of 50 mL for hydrothermal treatment at 170°C for 24 h. As the autoclave was cooled to room temperature naturally, the precipitates were washed with distilled water and absolute ethanol, and dried in air.[16]

Preparation of MoO_3/PANI: 0.15 g of α–MoO_3 nanorods was dispersed in 100 mL of 1 mol L^{-1} HCl solution by sonication treatment and then the mixture was cooled down to 0°C under stirring. 0.3 mL of aniline was dissolved in 100 mL of 1 mol L^{-1} HCl solution, and then transferred to the solution of ammonium persulfate(0.375 g) dissolved in 100 mL of 1 mol L^{-1}HCl solution in the beaker. The mixture solution above was cooled down to 0°C, then transferred to the suspension and kept at the temperature for 4 h under stirring. The precipitate was washed by distilled water and ethanol, and then dried at 40 °C for 24 h.

Preparation of Mo_2C catalysts: After the MoO_3/PANI hybrids were thermally treated at 850°C for 2 h at 10 % H_2/Ar gas flow, the Mo_2C-2 were obtained. The samples, obtained as the amount of aniline is changed to 0.2 and 0.4 mL, named as Mo_2C-1 and Mo_2C-3 respectively.

2.2 Structural Characterization

The morphology and size of the synthesized 3D architectures were characterized by scanning electron microscope [HSD/SU70] and an FEI Tecnai-F20 transmission electron microscope equipped with a Gatan imaging filter (GIF). The crystal structure of the sample was determined by X-ray diffraction (XRD) [D/max 2550 V, Cu Ka radiation]. XPS measurements were carried out using a spectrometer with Al Kα radiation (K-Alpha, Thermo Fisher Scientific Co.). The binding energy was calibrated with the C 1s position of contaminant carbon in the vacuum chamber of the XPS instrument (284.8 eV).

2.3 Electrochemical measurements

Electrochemical measurements were performed in a three-electrode system at an electrochemical station (CHI660D). The three-electrode configuration using an Ag/AgCl (KCl saturated) electrode as the reference electrode, a graphite rod as the counter electrode, and the carbon paper coated with catalyst was used as the working electrode. The working electrode was fabricated as follow: the catalyst was dispersed in N-methyl-2-pyrrolidone (NMP) solvent containing 7.5 wt% polyvinylidene fluoride (PVDF) under sonication, in which the weight ratio of the catalyst to PVDF is 8:1. Then the slurry was coated onto a piece of carbon paper (length×diameter×thickness = 6 cm×1 cm×0.03 cm). The effective loading area was about 1 cm^{-2} and the loading density of the catalyst was ~ 3 mg cm^{-2}. Linear sweep voltammetry with scan rate of 5 mV s^{-1} was conducted in 0.5 M H_2SO_4 (deaerated by N_2). All data have been corrected for a small ohmic drop based on impedance spectroscopy. In 0.5 M H_2SO_4, $E_{(RHE)} = E_{(SCE)} + 0.21$ V. All the potentials reported in our manuscript were calibrated to a reversible hydrogen electrode (RHE).

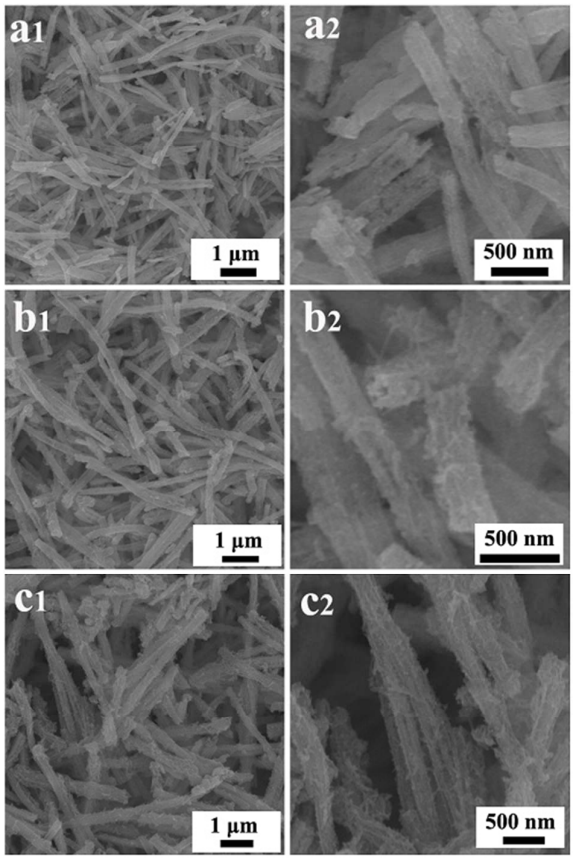

Figure 2 Typical SEM images of Mo_2C-based catalysts with different magnifications. a1-a_2) Mo_2C-1, b1-b2) Mo_2C-2, and c1-c2) Mo_2C-3.

3 Results and discussion

The phase purity and crystal structure of the final products were examined by XRD, as shown in Figure 1. The diffraction peaks located at 2θ = 34.4°, 38.0°, 39.4°, 52.1°, 61.5°, and 69.6° originate from (100), (002), (101), (102), (110) and (103) planes of β-Mo_2C (JCPDs PDF no. 35-0787). The signals from possible impurities such as MoO_3 and MoO_2 are not detected in all of the samples, indicating their high crystal purities. From Figure 1 we can also find that the diffraction peaks of the porous 1D Mo_2C-based catalysts are gradually broaden with the increase of the amound of PANI in precursors, suggesting that Mo_2C-3 has the smallest crystal size among the three samples. According to the Scherrer equation the calculated crystal sizes of Mo_2C nanocrystals in Mo_2C-1, Mo_2C-2 and Mo_2C-3 are 19.4, 12.5 and 9.6 nm, respectively. In addition, a broaden peak centred at 2θ = 25° in the XRD pattern of Mo_2C-3 reveals that Mo_2C-3 has relatively higher weight percentage of amorphous carbon materials than those of Mo_2C-1 and Mo_2C-2.

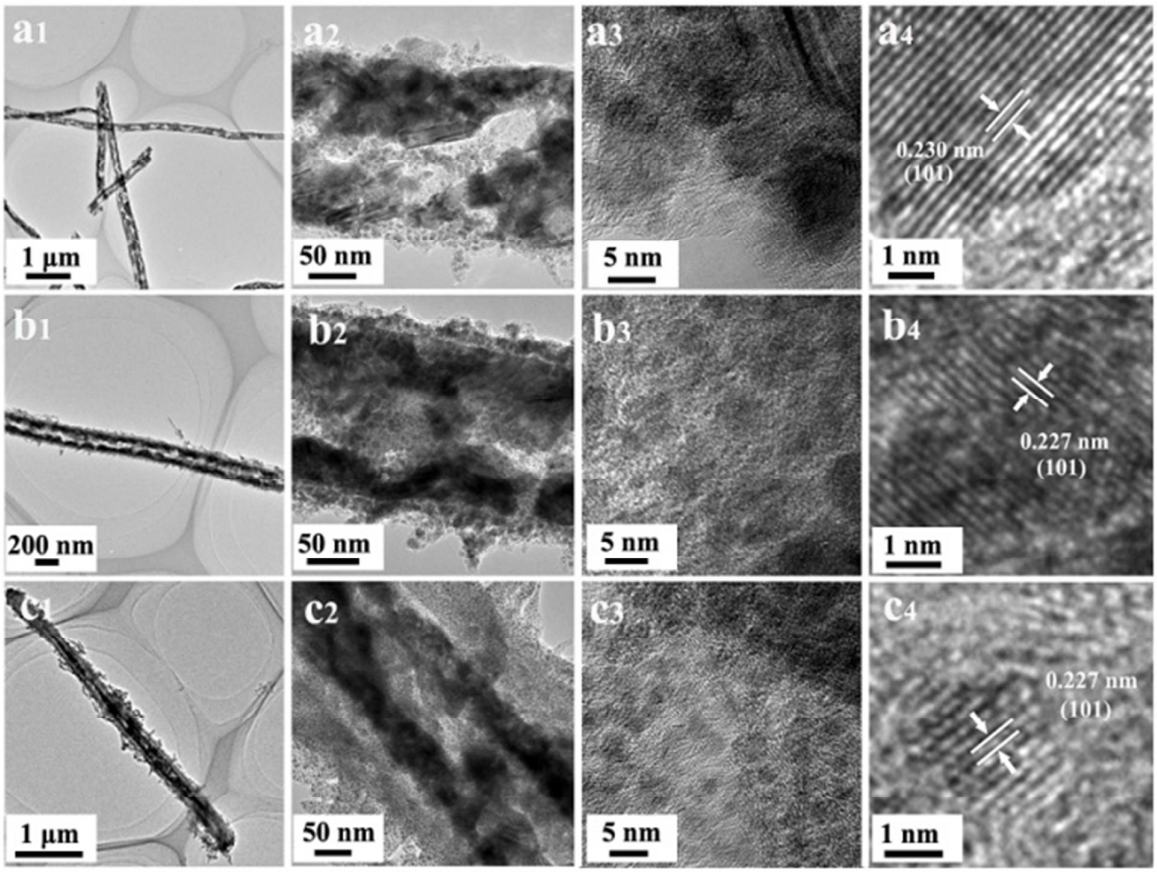

Figure 3 TEM images of Mo_2C-based catalysts with different magnifications. a_1-a_4) Mo_2C-1, b_1-b_4) Mo_2C-2, c_1-c_4) Mo_2C-3.

Figure 2 shows SEM images with different magnifications of Mo_2C-1, Mo_2C-2 and Mo_2C-3. From low-magnification SEM iamges (Figure 2a1–c1) it can be found that all the three electrocatalysts have one-dimensional (1D) shapes with lengthes in several micrometers. However, the diameters of the three electrocatalysts are quite different. As shown in Figure 2a1–c1, the diameters of Mo_2C-1, Mo_2C-2, and Mo_2C-3 are about 200, 250, and 300 nm, respectively, with respect to the amount of PANI in the precursors. It demonstrates that larger amount of PNAI leads to larger diamerter of the 1D Mo_2C electrocatalysts. Interestingly, many mesopores can be observed along the axes of 1D Mo_2C-1 and Mo_2C-2 electrocatalysts, as shown in the high-magnification SEM images (Figure 2a2 and 2b2). However, there are less mesopores are in Mo_2C-3 (Figure 2c2). Moreover, the ends of most of Mo_2C-1 and Mo_2C-2 are open, as shown in Figure 2a2 and 2b2. Thus Mo_2C-1 and Mo_2C-2 have porous and tubular characteristics, which facilitate more active sites to expsoe to the electrolyte directly, and in turn boost the HER activities of the electrocatalysts. The formation of pores is related to the growth mechanism of the Mo_2C nanoparticles and the amount of PANI in the precursors. At a high temperature, MoO_3 is easily sublimated and its diffusion rate is faster than that of the PANI. With the in situ solid state reaction between MoO_3 and PANI being proceeded, the Mo_2C nanoparticles are produced, accompanying the formation of a hollow region in the center of the products. At the same time, smaller amount of PANI covered over the MoO_3 surfaces in the precursors will lead to more MoO_3 vapors escaped out to environment and does not react with PANI, leaving more pores in the final products. The energy dispersive spectrometry (EDS) is conducted to determine the composition content of the Mo_2C electrocatalysts. Statistical results show that the contents of Mo_2C in Mo_2C-1, Mo_2C-2 and Mo_2C-3 are 61.9, 67.6 and 41.3 wt%, respectively.

The structures of Mo_2C-1, Mo_2C-2 and Mo_2C-3 were further analyzed by TEM observations. The low magnification TEM images (Figure $3a_1$–$3c_1$) show that Mo_2C-1 and Mo_2C-2 porous and tubular features, whereas the features are not obvious for Mo_2C-3, in consistent with the SEM observations. As expected, the thickness of amorphous carbon layers in the Mo_2C-based electrocatalysts is increased with the increase of the amount of PANI precursors. As shown in Figure $3a_2$–$3c_2$, the thickness of the amorphous carbon layers of Mo_2C-1, Mo_2C-2 and Mo_2C-3 are in the range of 5–25, 25–50 and 70–130 nm, respectively. The presence of the carbon layer in the electrocatalysts is in favor of the improvement of the conductivity for HER. However, too large thickness will reduce the number of the active sites exposed to electrolyte. From these figures, it can be also found that there are many Mo_2C nanoparticles in the inner walls and even in outside carbon layers of Mo_2C-1, Mo_2C-2, and Mo_2C-3. The high-magnification TEM images (Figure $3a_3$–$3c_3$) show that the sizes of Mo_2C nanoparticles in Mo_2C-1, Mo_2C-2, and Mo_2C-3 are about 8–25, 5–20 nm and 3–11 nm, respectively. The lattice spacings labeled in Figure $3a_4$–$3c_4$ are about 0.230, 0.227 and 0.227 respectively, corresponding to (101) crystal planes of Mo_2C. The results above demonstrate that our Mo_2C-based electrocatalysts are composed of crystalline Mo_2C nanoparticles and amorphous carbon layers. Furthermore, the thickness of carbon layers and crystal size of Mo_2C in the electrocatalysts can be tuned by the amount of PANI in the precursors.

To probe the electronic structures on the surface of the catalysts, the samples were analyzed by X-ray photoelectron spectroscopy (XPS) (Figure S1). The peaks at binding energies of 228.5 and 231.6 eV in the high resolution of Mo 3d XPS spectrum (Figure S1(a)) can be assigned to $3d_{5/2}$ and $3d_{3/2}$ of $Mo^{(II)}$, respectively.[2b, 2c] Other peaks at the binding energies of 232.4 and 235.5 eV for $Mo^{(VI)}$ coming from MoO_3 are also observed.[2b, 2c] In consistency with the previous studies, the surfaces of the Mo_2C catalysts can be contaminated with molybdenum oxides (MoO_2 and MoO_3) when exposed to air for a period of time.[2b, 2c, 6] Figure S1(b) shows high-resolution C 1s XPS spectrum, in which the peak indicates that C–O (at 286.0 eV) groups exist in the layers of the samples.

The electrocatalytic HER activities of our Mo_2C based electrocatalysts were investigated in 0.5 M H_2SO_4 solution using a three-electrode setup. For comparison, the HER performance of Pt was also tested. Figure 4a shows the polarization curves of the catalysts with a sweep rate of 5 mV s^{-1}. Pt exhibits expected HER activity with nearly zero onset overpotential and high current density. All of our Mo_2C-based electrocatalysts show small onset overpotentials and high current densities at moderate overpotentials. For driving cathodic current densities of 1 mA cm^{-2}, Mo_2C-1, Mo_2C-2 and Mo_2C-3 only need overpotentials of 63, 49 and 30 mV, respectively (Table S1).† Beyond the onset overpotentials, the current densities for all the three catalysts are increased rapidly. Notably, Mo_2C-2 exhibits superior HER activity than Mo_2C-1 and Mo_2C-3. For example, for driving cathodic current densities of 10 and 50 mA cm^{-2}, Mo_2C-2 shows only overpotentials of 115 and 154 mV respectively, whcih are smaller than those of Mo_2C-1(134 and 172 mV) and Mo_2C-3 (146 and 201 mV). Furthermore, the cathodic current density measured by Mo_2C-2 electrode can be up to 216.8 mA cm^{-2} at η= 200 mV, which is the largest value among the reported Mo_2C catalysts and ever better than the lithiation-treated S-MoS_2 (Li-MoS_2) and the MoP thin film on the Ti foil in acidic solutions.[2f, 3e] † The detail comparison is shown in Table S2.†

For further study of HER activity of the Mo_2C based electrocatalysts, Tafel plots were fitted to Tafel equation ($\eta = a + b\log|j|$), where b is the Tafel slope. As shown in Figure 4b, the Pt catalyst exhibits a Tafel slope of 30 mV dec^{-1}, which is consistent with the reported values. The Tafel slopes of the Mo_2C-1, Mo_2C-2, and Mo_2C-3 are 57.5, 57.6 and 74 mV $decade^{-1}$, respectively. The Tafel slopes for the 1D Mo_2C catalysts do not match with the expected Tafel slopes of 29, 38, and 116 mV $decade^{-1}$, suggesting the HER proceeds via a Volmer–Heyrovsky mechanism.[19-21] The exchange current density (j_0) is an important factor to evaluate the HER activity of the catalysts. the value of the exchange current density can be obtained from Tafel plots by using extrapolation methods (Figure S2).† When extrapolating the Tafel plot to an overpotential of 0 mV, the exchange current density of Mo_2C-2 is estimated to be 102.3 μA cm^{-2}, which is higher than those of Mo_2C-1 (50.6 μA cm^{-2}), Mo_2C-3 (76.6 μA cm^{-2}) and most Mo_2C-based electrocatalysts previously reported, as shown in Table S2.†

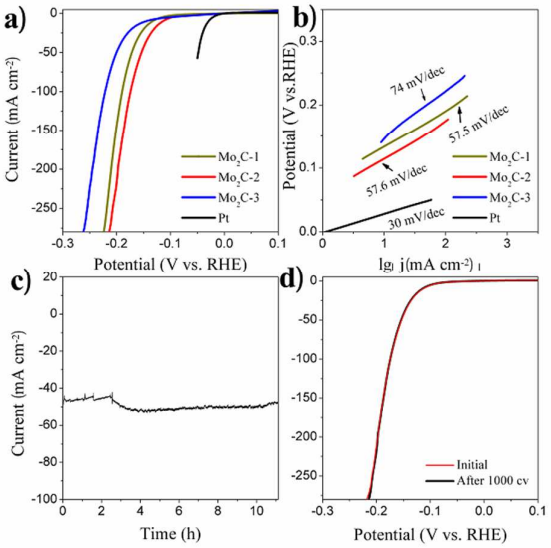

Figure 4 a) Polarization curves and b) Tafel plots of Mo_2C-1, Mo_2C-2, Mo_2C-3 and Pt, c) Cycling stability of Mo_2C-2 at an overpotential of 200 mV, d) the polarization curves before and after potential sweeps for 1000 cycles in 0.5 M H_2SO_4 solution.

The results above demonstrate that our Mo_2C based electrocatalysts (Mo_2C-1 and Mo_2C-2) exhibit excellent HER activity including small onset overpotentials, large current densities at moderate overpotentials and large exchange current density, superior to most Mo_2C electrocatalysts previously reported (Table S2).† It may be related to the following factors. (i) The porous and tubular characteristics of our Mo_2C-1 and Mo_2C-2 greatly favor in the contact of the active sites with electrolyte efficiently, leading to a significant acceleration of

the interfacial electrocatalytic reactions. (ii) The presence of the carbon layers in the catalysts can improve the whole conductivity of the catalyst, and thereby increase the charge transfer rate during the HER process. In order to clarify it, electrochemical impedance spectroscopy (EIS) analysis were analysed at different overpotentials. Figure S3 shows Nyquist plots of impedance spectroscopy of Mo_2C-1, Mo_2C-2 and Mo_2C-3 at different overpotentials.† As fitted from the experimental data by a two time-constant model (the inset in Figure S3a) the transfer resistances of these Mo_2C catalysts can be obtained, and the values are listed in Table S3.† It can be found that Mo_2C-1, Mo_2C-2 and Mo_2C-3 have lower charge-transfer resistance than those of most Mo_2C electrocatalysts previously reported.

Notably, Mo_2C-2 exhibits superior HER activities to Mo_2C-1 and Mo_2C-3, which may be related to its larger active areas and larger content of Mo_2C. On one hand, there are smaller contents of Mo_2C in Mo_2C-1 and Mo_2C-3 than in Mo_2C-2, evidenced by EDS measurements. Due to small difference in the catalyst size, the higher content of Mo_2C implys Mo_2C-2 has more active sites for HER. On the other hand, the carbon layers are too thick in Mo_2C-3, which impedes active sites to contact with electrolytes to some degree. The electrochemical double-layer capacitances (C_{dl}) can be measured to estimate the effective active area of our Mo_2C -based catalysts using a simple cyclic voltammetry method (Figure 5). As shown in Figure 5d, Mo_2C-2 exhibits the C_{dl} value of 83.7 mF, larger than Mo_2C-1 (58 mF) and Mo_2C-3 (50.9 mF). This result reveals that Mo_2C-2 has the largest effective active area among the Mo_2C-based catalysts, which contributes to its superior HER activity.

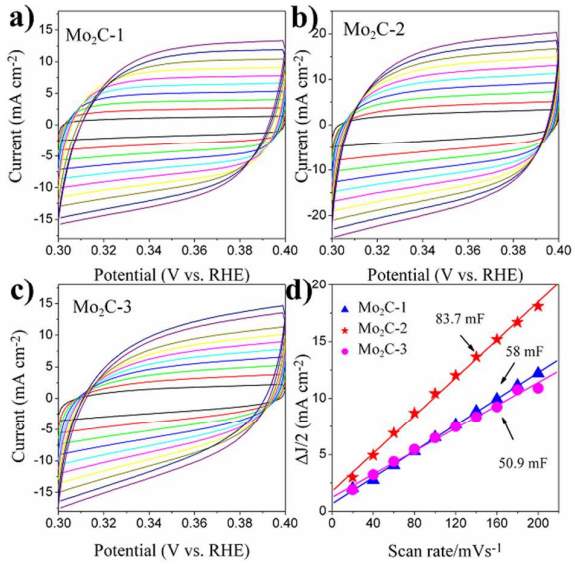

Figure 5 Cyclic voltammograms performed at various scan rates (20, 40, 60 mV s^{-1}, etc.) in the region of 0.3–0.4 V vs. RHE for a) Mo_2C-1, b) Mo_2C-2 and c) Mo_2C-3. d) The differences in current density ($\Delta J = J_a - J_c$) at 0.35 V vs. RHE plotted against scan rate fitted to a linear regression allows for the estimation of C_{dl}.

Durability is also a key factor for a good catalyst. The long-term durability of Mo_2C-2 was examined by electrolysis at η= 200 mV for 40 000 s in 0.5 M H_2SO_4. As shown in Figure 4c, the Mo_2C-2 electrode can be holding a high current density of 50 mA cm^{-2} at the given potential for a long time without a significant degradation. The stability of Mo_2C-2 in the acidic media was also investigated by sweeping the catalysts for 1000 cycles. We measured 1000 continuous cyclic voltammograms between -0.3 and +0.2 V vs RHE (without *iR* corrected) at 100 mVs^{-1}. After the cycles, the negligible current loss is observed, as shown in Figure 4d. Thus, our porous 1D Mo_2C catalysts have excellent long-term stability for HER.

4 Conclusions

Porous 1D Mo_2C based catalysts with tubular features are fabricated by *in situ* solid reactions using MoO_3/PANI nanorods as precursors. The crystal size of Mo_2C and the thickness of the carbon layers in 1D Mo_2C nanostructures can be tuned by the amount of PANI in the precursors. Due to the good conductivity, porous and tubular characteristic, and large active area, the Mo_2C-based electrocatalyst with moderate thickness of the carbon layers exhibits superior catalytic activities for HER to most Mo_2C based electrocatalysts previously reported. For driving cathodic current densities of 10 mA cm^{-2} in 0.5 M H_2SO_4 solution, it only needs an overpotential of 115 mV vs RHE. Our results demonstrate that the porous 1D Mo_2C catalysts are very promsing for practical applications.

Acknowledgements

We thank the National Natural Science Foundation of China (Grant Nos. 51272050 and 21271053), the Innovation Foundation of Harbin City (2012RFXXG096), and also the 111 project (B13015) of Ministry Education of China to the Harbin Engineering University.

Notes and references

1 a) N. S. Lewis and D. G. Nocera, *Proc. Natl. Acad. Sci. USA*, 2006, **103**, 15729; b) T. R. Cook, D. K. Dogutan, S. Y. Reece, Y. Surendranath, T. S. Teets and D. G. Nocera, *Chem. Rev.*, 2010, **110**, 6474 – 6502; c) M. G. Walter, E. L. Warren, J. R. McKone, S. W. Boettcher, Q. X. Mi, E. A. Santori and N. S. Lewis, *Chem. Rev.*, 2010, **110**, 6446; d) N. S. Lewis, *Science*, 2007, **315**, 798–801.

2 a) B. Himmemann, P. G. Moses, J. Bonde, K. P. Jørgensen, J. H. Nielsen, S. Horch, I. Chorkendorff and J. K. Nørskov, *J. Am. Chem. Soc.,* 2005, **127**, 5308; b) H. Vrubel, D. Merki and X. Hu, *Energy Environ. Sci.*, 2012, **5**, 6136; c) J. Kibsgaard, Z. Chen, B. N. Reinecke and T. F. Jaramillo, *Nat. Mater.,* 2012, **11**, 963; d) J. F. Xie, H. Zhang, S. Li, R. X. Wang, X. Sun, M. Zhou, J. F. Zhou, X. W. Lou and Y. Xie, *Adv. Mater.,* 2013, **25**, 5807; e) S. Zhuo, Y. Xu, W. Zhao, J. Zhang and B. Zhang, *Angew. Chem. Int. Ed.,* 2013, **52**, 8602; f) H. T. Wang, Z. Y. Lu, D. S. Kong, J. Sun, T. M. Hymel, and Y. Cui, *ACS Nano*, 2014, **8**, 4940; g) K. Zhang, Y. Zhao, S. Zhang, H. L. Yu, Y. J. Chen, P. Gao and C. L. Zhu, *J. Mater. Chem. A,* 2014, **2**, 18715.

3 a) P. Xiao, M. A. Sk, L. Thia, X. M. Ge, R. J. Lim, J. Y. Wang, K. H. Lim and X. Wang, *Energy Environ. Sci.,* 2014, **7**, 2624; b) Z. C. Xing, Q. Liu, A. M. Asiri and X. P. Sun, *Adv. Mater.,* 2014, **26**, 5702; c) X. B. Chen, D. Z. Wang, Z. P. Wang, P. Zhou, Z. Z. Wu and F. Jiang, *Chem. Commun.,* 2014, **50**, 11683; d) W. Cui, Q. Liu, Z. Xing, A. M. Asiri, K. A. Alamry and X. P. Sun, *Appl. Catal. B,* 2015, **164**, 144; e) J. Kibsgaard and T. F. Jaramillo, *Angew. Chem. Int. Ed.,* 2014, **53**, 14433.

4 J. Xie, S. Li, X. Zhang, J. Zhang, R. Wang, H. Zhang, B. Pan and Y. Xie, *Chem. Sci.*, 2014, **5**, 4615.
5 D. H. Youn, S. Han, J. Y. Kim, J. Kim, H. Park, S. H. Choi and J. S. Lee, ACS Nano, 2014, **8**, 5164.
6 H. Vrubel and X. Hu, *Angew. Chem. Int. Ed.*, 2012, **51**, 12703.
7 W. F. Chen, C. H. Wang, K. Sasaki, N. Marinkovic, W. Xu, J. T. Muckerman, Y. Zhu and R. R. Adzic, *Energy Environ. Sci.*., 2013, **6**, 943.
8 W. F. Chen, J. T. Muckerman and E. Fujita, *Chem. Commun.*, 2013, **49**, 8896.
9 L. Liao, S. Wang, J. Xiao, X. Bian, Y. Zhang, M. D. Scanlon, X. Hu, Y. Tang, B. Liu and H. H. Girault, *Energy Environ. Sci.*, 2014, **7**, 387.
10 L. F. Pan, Y. H. Li, S. Yang, P. F. Liu, M. Quan and H. G. Yang, *Chem. Commun.*, 2014, **50**, 13135.
11 C. Wan, Y. N. Regmi and B. M. Leonard, *Angew. Chem. Int. Ed.*, 2014, **53**, 6407.
12 W. Cui, N. Cheng, Q. Liu, C. Ge, A. M. Asiri and X. Sun, ACS Catal. 2014, **4**, 2658.
13 C. J. Ge, P. Jiang, W. Cui, Z. H. Pu, Z.C. Xing, A. M. Asiri, A. Y. Obaid and X. P. Sun, J. Tian, *Electrochim. Acta*, 2014, **134**,182.
14 P. Xiao, Y. Yan, X. M. Ge, Z. L. Liu, J. Y. Wang and X. Wang, *Appl. Catal. B: Environ.,* 2014, **154**, 232.
15 P. Xiao, X. M. Ge, H. B. Wang, Z. L. Liu, A. Fisher, and X. Wang, *Adv. Funct. Mater.*, 2015, **25**, 1520.
16 K. Zhang, Y. Zhao, D. Y. Fu and Y. J. Chen, *J. Mater. Chem. A,* 2015, **3**, 5783.
17 Q. S. Wang, Z. Y. Lei, Y. J. Chen, Q. Y. Ouyang, P Gao, L. H. Qi, C. L. Zhu and J. Z. Zhang, *J. Mater. Chem. A,* 2013, **1**, 11795.
18 K. Zhang, W. Yang, C. Ma, Y. Wang, C. W. Sun, Y. J. Chen, P. Duchesne, J. G. Zhou, J. Wang, Y. F. Hu, M. N. Banis, P. Zhang, J. Q. Li, F. Li and L. Q. Chen, *NPG Asia Mater.,* 2015, **7**, e153.
19 B. E., Conway and B. V. Tilak, *Electrochim. Acta*, 2002, **47**, 3571.
20 Y. G. Li, H. L. Wang, L. M. Xie, Y. Y. Liang, G. S. Hong and H. J. Dai, *J. Am. Chem. Soc.,* 2011, **133**, 7296.
21 J. F. Xie, J. J. Zhang, S. Li, F. Grote, X. D. Zhang, H. Zhang, R. X.Wang, Y. Lei, B. C. Pan and Y. Xie, *J. Am. Chem. Soc.,* 2013, **135**, 17881.